THE JOURNAL OF PHYSICAL CHEMISTRY B

Article

pubs.acs.org/JPCB

Distinguishing Single DNA Nucleotides Based on Their Times of Flight Through Nanoslits: A Molecular Dynamics Simulation Study

Brian R. Novak,[†] Dorel Moldovan,*[,†] Dimitris E. Nikitopoulos,[†] and Steven A. Soper[‡,§,∥]

[†]Department of Mechanical and Industrial Engineering, and Center for Computation and Technology, Louisiana State University, Baton Rouge, Louisiana 70803, United States

[‡]Department of Chemistry, and [§]Department of Biomedical Engineering, University of North Carolina, Chapel Hill, North Carolina 27599, United States

[∥]North Carolina State University, Raleigh, North Carolina 27695, United States

Supporting Information

ABSTRACT: Transport of single molecules in nanochannels or nanoslits might be used to identify them via their transit (flight) times. In this paper, we present molecular dynamics simulations of transport of single deoxynucleotide 5′-monophoshates (dNMP) in aqueous solution under pressure-driven flow, to average velocities between 0.4 and 1.0 m/s, in 3 nm wide slits with hydrophobic walls. The simulation results show that, while moving along the slit, the mononucleotides are adsorbed and desorbed from the walls multiple times. For the simulations, the estimated minimum slit length required for separation of the dNMP flight time distributions is about 5.9 μm, and the minimum analysis time per dNMP is about 10 μs. These are determined by the nature of the nucleotide−wall interactions, channel width, and by the flow characteristics. A simple analysis using realistic dNMP velocities shows that, in order to reduce the effects of diffusional broadening and keep the analysis time per dNMP reasonably small, the nucleotide velocity should be relatively high. Tailored surface chemistry could lead to further reduction of the analysis time toward its minimum value for a given driving force.

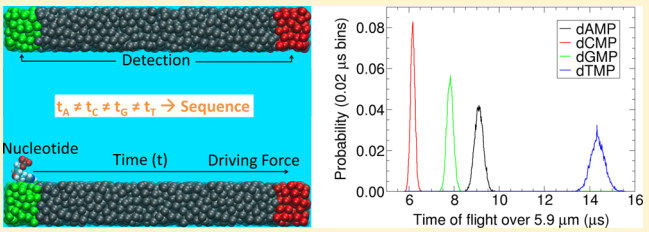

INTRODUCTION

Various technologies are being developed for fast and low-cost sequencing of linear heteropolymers such as DNA. Several approaches are based on the use of nanopores and distinguishing the DNA nucleotides using blockage currents,[1] transverse conductance,[2] transverse differential conductance,[3] optical recognition,[4] or using sequence-specific hysteresis effects observed when applying an ac electric field.[5] Some approaches use the intact polymer,[6] and others use individual nucleotides of a sequentially disassembled polymer.[7] Nanopores that have been considered include the membrane protein α-hemolysin or pores constructed from other materials such as a polymer, silicon nitride,[8] or graphene.[9−17] Another approach is to distinguish the monomers of an enzymatically disassembled DNA strand created from fluorescently labeled nucleotides with color discrimination.[18−20] Alternative fluorescence-based strategies have been proposed that follow incorporation events of fluorescently labeled nucleotide triphosphates by polymerases.[21]

In this study, we introduce an alternative approach for heteropolymer sequencing based on enzymatic disassembly of a single polymer into individual monomers followed by the measurement of the flight (transit) time of each monomer as it passes through a nanochannel or nanoslit. In practice, the time of flight can be determined by monitoring the passing of each monomer at two or more locations along the channel. The basic hypothesis is that individual monomers in solution moving through a nanochannel and interacting with its walls will experience transit time distributions that are dependent upon their molecular identity, their size, and the chemical identity of the surface of the channel. This time-of-flight-based approach is similar to chromatography. Mononucleotides can be separated by chromatography,[22−24] so this approach should work in theory.

For DNA, mononucleotides would be generated by subjecting an intact DNA molecule to an enzyme poised in a solid-phase nanoreactor. The enzyme, such as λ-exonuclease, would be covalently attached to a pillar, which would be positioned at the input end of the nanosensor. Due to the processive nature of this enzyme, single mononucleotides would be shuttled into the nanosensor with minimal amounts of diffusional misordering. If errors due to stochastic misordering were to occur, they could be mitigated by analyzing each biopolymer multiple times to generate a consensus sequence.

The nanochannels for this system would be constructed from a polymer material using nanoimprint lithography.[25] A likely candidate for the polymer is poly(methyl methacrylate) (PMMA). PMMA is a transparent thermoplastic that can be molded into nanostructures using nanoimprint lithography, and its surface chemistry can be modified.[26−29] PMMA channels with widths smaller than 10 nm have been constructed using nanoimprint lithography.[30]

Received: September 24, 2012
Revised: February 6, 2013

   dx.doi.org/10.1021/jp309486c | J. Phys. Chem. B XXXX, XXX, XXX−XXX

In a sequencing device using the flight time strategy, monomer–wall interactions must be tailored such that the flight time distributions of each monomer type can be separated over minimal distances. The ideal surface type would be one to which the monomers are slightly attracted to the walls with different attraction strengths for each monomer type. If any monomer type was strongly attracted to the surfaces then it could adsorb to the walls for long periods of time, which would lead to a broader time-of-flight distribution and the possibility of other monomers passing it before it clears the last sensor.

The detection of the mononucleotides might be accomplished through the use of nanoelectrodes. With an electrode–electrode gap of about the length of a nucleotide, tunneling current can be used to detect single nucleotides.[31]

The goals of this work were to study the feasibility of separating the time-of-flight distributions of the four DNA nucleotides monophosphates (dNMPs) and to develop a fundamental understanding of the characteristics of the dynamics and adsorption/desorption statistics of the dNMPs interacting with the walls of a nanoslit with and without the flow of the aqueous solution. Understanding the dNMP–wall interactions can ultimately provide insights, and guidance, to experimentalists designing the surface chemistry of nanochannel walls.

Molecular dynamics (MD) simulations were used to address the above goals. Both equilibrium and nonequilibrium (flow) MD simulations of dNMPs in nanoslits were performed with LAMMPS.[32] The simulations consisted of individual dNMPs in aqueous solution, with a total ion concentration of sodium chloride set at 89 mM, that filled the space between two atomically smooth walls composed of tethered, disordered Lennard-Jones carbon-like atoms with the same number density as the non-hydrogen atoms in amorphous PMMA.

METHODS

The CHARMM27 force field[33] was used for the dNMP and ion interactions with the rigid CHARMM TIP3P model for water. The short-range cutoff for the electrostatics was 1.0 nm. The Lennard-Jones interactions were switched to zero in the interval between 0.8 and 1.0 nm. The three-dimensional particle–particle particle–mesh method corrected for slab geometry,[34] with the length in the nonperiodic direction 3 times the simulation box length in that direction, was used for long-range electrostatic interactions.

The deoxynucleotide monophosphates or dNMPs (dAMP, dCMP, dGMP, dTMP) with a phosphate group on their 5′ end can be produced from the cutting of an intact double-stranded DNA using, for example, λ-exonuclease. On the basis of the optimal pH for enzyme activity of 7.5, the phosphates of the dNMPs were simulated as nonprotonated because their pK_a's are approximately 6.8,[35] giving them a net charge of $-2e$, where e is the electron charge. The CHARMM27 topology file does not contain a terminal segment for DNA with a nonprotonated phosphate on the 5′ end. Patches are used to modify an existing topology by adding or subtracting atoms and modifying partial charges. The topology file does contain terminal patches for DNA with a protonated phosphate on the 5′ end, a protonated phosphate on the 3′ end, and a nonprotonated phosphate on the 3′ end. Therefore, the difference in partial charges on the affected atoms between the nonprotonated and protonated 3′ versions was added to the partial charges for the nonprotonated 5′ versions. The affected atoms included only the phosphate group and the carbon atom directly attached to it. The patch added to the CHARMM topology file is included in the Supporting Information. Figure 1 shows dNMPs with all four of the termini and the affected atoms labeled.

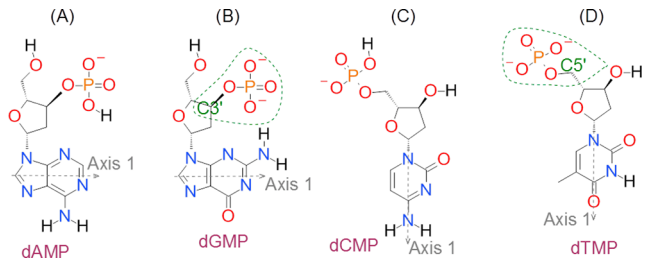

Figure 1. dNMP structures containing the four nucleobases: (A) protonated 3′ dAMP; (B) nonprotonated 3′ dGMP; (C) protonated 5′ dCMP; (D) nonprotonated 5′ dTMP. The differences between the partial charges on the encircled atoms in structure B and the corresponding atoms in structure A were applied to structure C to get the partial charges on the encircled atoms in structure D. The only structural difference between the encircled atoms in structures B and D is at the C3′ and C5′ atoms. Structures like D with the four different nucleobases were used in the simulations. The identity of the nucleobase does not affect the partial charges on the phosphate group. The axes labeled axis 1 on the nucleobases were used in the analysis of dNMP adsorption and desorption to the slit walls and are discussed in the Results and Discussion section.

The slit walls were defined by two planes, parallel to the xy plane and located at $z = \pm 1.5$ nm; the centers of the wall atoms are located at $z \leq -1.5$ nm (bottom) and $z \geq 1.5$ nm (top). The slit walls were constructed by performing a simulation of a bulk fluid composed of atoms with Lennard-Jones 12–6 parameters for a carbon atom ($\varepsilon_{carbon-carbon}$ = 0.11 kcal/mol, $\sigma_{carbon-carbon}$ = $0.4/2^{1/6}$ nm). The mass of the atoms was increased from 12.011 to 14.30226 amu so that it was equal to the mass of the average mass of the atoms in a united atom (no hydrogen atoms, but increased mass of atoms that would have hydrogen atoms attached to them) representation of PMMA. This simulation was run at 5000 K, to ensure that it was a fluid, and at a density near that of amorphous PMMA.[36] The size of the simulation box in the x and y directions was chosen to be 5.0 nm in order to match the desired size of the slit walls. The slit wall initial configurations were taken from $5.0 \times 5.0 \times 1.2$ nm^3 rectangular regions of this fluid. If the atom centers were inside the rectangular region, they were included in the wall. This resulted in surfaces that were atomically smooth (roughness less than the size of an atom), but heterogeneous. Each set of slit walls was taken from different times during the fluid simulation spaced 10 ps apart. A slit width of 3 nm was chosen to avoid wasting simulation time allowing the dNMPs to diffuse around in the center of the slit for long periods, although real channels with dimensions smaller than 5 nm have been fabricated.[37] It should also be noted that using small, completely hydrophobic nanoscale geometries is not practical due to the difficulty for water to enter them. The slit walls were not chosen to be physically realistic, but as a simple system for this initial study. Future work will focus on more realistic walls.

Once the walls were constructed, the dNMPs were moved between the slit walls and water and ions were added using VMD.[38] NPT simulations could not be performed in LAMMPS for the geometry that was used, so the amount of water was determined by trial and error. The *Solvate* function in VMD was used to add water with the settings: boundary = 2.4, x and y

dx.doi.org/10.1021/jp309486c | J. Phys. Chem. B XXXX, XXX, XXX–XXX

bounds = ±25.65 Å, z bounds = ±15 Å. These settings were determined by trial and error to get a reasonable bulk density of water (center of slit) in equilibrium simulations containing only water and the slit walls. The equilibrium bulk water density was about 1.015 g/cm^3. After the dNMP was solvated, four water molecules were removed and replaced with three sodium ions and one chloride ion using the *Autoionize* function in VMD. The simulation system used for both the equilibrium and nonequilibrium simulations and the chemical structure of DNA is shown in Figure 2.

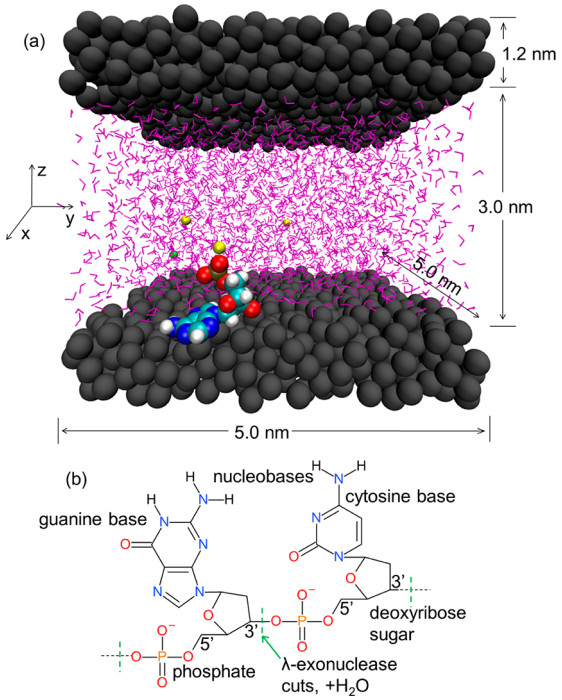

Figure 2. (a) Simulation system containing water, sodium chloride, and a dNMP in a nanoslit. Gray spheres represent wall atoms, green represents chloride, tan represents phosphorus, yellow represents sodium, red represents nonwater oxygen, white represents nonwater hydrogen, cyan represents nonwall carbon, blue represents nitrogen, and purple represents water molecules. Some of the wall atoms are not shown for clarity. There are periodic boundary conditions in the x and y directions. (b) Two dNMPs (only polar hydrogens are shown). Single ring pyrimidine (C, T) and two ring purine (A, G) nucleobases are attached to the sugar–phosphate backbone. λ-Exonucleases can digest one strand of a double-stranded DNA one dNMP at a time starting from the 5′ end and leaving the phosphate on the 5′ end of each released dNMP.

The following describes the methods and general parameters used in carrying out the simulations. The wall atoms were attached to their initial positions by springs with spring constants of 83 860 kcal/mol·nm^2. For the flow simulations, only the wall atoms were thermostatted at 300 K using a Berendsen thermostat with a time constant of 0.1 ps. The fluid temperatures during flow at steady state were about 3 K higher than the temperature of the thermostatted walls due to heating of the fluid by viscous flow. For the equilibrium simulations, an additional thermostat was used for the fluid with the same time constant. For each dNMP, three or four simulations were run with different wall configurations to reduce any bias due to particular wall configurations. Flow was induced by applying a constant body force in the x direction (see Figure 2), f_i, to each atom. The magnitude of f_i was chosen such that $f_i = m_i a$, where m_i is the mass of atom i and a is the acceleration, chosen the same for all atoms. This approach is an approximation to pressure-driven flow[39,40] or flow generated by capillary forces.[41] The pressure gradient along the direction of flow due to the applied forces f_i on all n atoms of the fluid is given by $dp/dx = \sum_{i=1}^{n} f_i/(A_{fluid}L_{box})$, where L_{box} is the length of the simulation box along the direction of the externally applied forces (x) and A_{fluid} is the area of the fluid in the plane perpendicular to the direction of the applied forces (yz plane). By choosing a = 263.592 nm/ns^2, and using the characteristic values for the parameters describing the simulation system (i.e., the number of atoms in the flow region and their mass, the area perpendicular to the flow, and the length of the simulation box) the pressure gradient that drives the flow in the nanoslit is about dp/dx = 2.836 bar/nm. The applied forces generate an approximately parabolic velocity profile across the z direction characterized by a maximum flow velocity of about 1.5 m/s. Simulation at such high velocities relative to velocities typical of nanoscale flows is necessary in MD simulations due to the relatively short time that is accessible, usually just few hundred nanoseconds. As discussed later, despite the very high velocities, the characteristic parameters describing the adsorption and desorption of dNMPs to and from the wall do not seem to be affected substantially by the flow. The first 15 ns of each flow simulation were discarded from the analysis to allow for steady-state conditions to be achieved. In the equilibrium simulations, a 1 ns equilibration period was discarded.

RESULTS AND DISCUSSION

Equilibrium Simulations and Adsorption Free Energy.

The goal of the equilibrium simulations was to investigate the mechanism and the energetics of individual dNMPs adsorption and desorption in the absence of flow. For each dNMP several simulations were run with different wall configurations (see Table 3). Each simulation lasted for about 65 ns, while the total simulation time for all four dNMPs and all of the various wall configurations was about 966 ns. The interaction of individual dNMPs with the slit walls is best described by their free energy profiles across the nanoslit. The free energy difference relative to a reference state, ΔF, as a function of a reaction coordinate (potential of mean force or PMF) is related to the probability, Pr, of the dNMP being located at a given value of the reaction coordinate. Because the probability for a dNMP to be adsorbed or desorbed from a nearly smooth surface was of interest, the reaction coordinate was taken as the distance, d_w, of the dNMP center of mass from the nearest slit wall plane located at $z = \pm 1.5$ nm. Using the values of $\Pr(d_w)$, the free energy profile is given by

$$\Delta F(d_w) = -kT \ln\left[\frac{\Pr(d_w)}{\Pr(d_{w,ref})}\right] \quad (1)$$

where k is Boltzmann's constant, T is the temperature, and $d_{w,ref}$ is the reference state chosen far from the wall in the center of the nanoslit ($z = 0$).

During the equilibrium simulations, all four dNMPs adsorbed and desorbed from the wall surface multiple times; therefore, eq 1 could be applied directly. Biased equilibrium simulations, such as umbrella sampling,[42−44] would be required to calculate the free energy in cases when dNMPs adsorb onto the slit surface for time periods comparable to the total simulation time (e.g., longer than a few nanoseconds). The multiple

dx.doi.org/10.1021/jp309486c | J. Phys. Chem. B XXXX, XXX, XXX−XXX

adsorption and desorption events also allowed for different adsorption sites on the heterogeneous surfaces to be sampled, so the ΔF in eq 1 is an average over those different sites. In fact, the dNMPs were mobile in the directions tangential to the wall plane even when adsorbed to a wall which allowed them to sample more of the wall surface. This is an indication that there are not any strong adsorption sites for the dNMPs on the wall surfaces and that there is little variation in adsorption strengths across the surfaces. As discussed in the Introduction, these are characteristics of the wall surfaces that are desired in order to make time-of-flight-based sequencing feasible. However, the wall surfaces are not made of a real material and are smoother than a real surface. Carr et al. found that adsorption at different sites on amorphous silica surfaces varied in strength from 0 to 10 kT.[43] The variation of dNMP adsorption strengths on PMMA surfaces is the subject of future work.

Figure 3 shows the profiles of the free energy as function of d_w for all four dNMPs. The profiles are similar and are characterized by the presence of well-defined minima. The existence of potential wells with depths of at most a few times the thermal energy, kT, reflects the fact that the dNMPs adsorb to the hydrophobic walls, but not strongly. The minima for the four curves are approximately located at the same distance, about 0.475 nm from the wall. As discussed in the next section, when dNMPs are adsorbed to the wall and are located in their minimum free energy state two of their main molecular units, the nitrogenous base and the sugar group, are in similar geometrical arrangement with respect to the wall surface, and therefore, they all have their center of mass located at about the same distance from the wall. All four curves show the presence of small barriers, of up to kT, located between the adsorption region and the bulk solvent close to the center of the slit. Here we define the adsorption region as the region close to the wall in which the dNMP experience pulling force toward the minima of their potential well. As seen in Figure 3 the outward extent of the adsorption regions for the four dNMPs can be delimited by the locations of the corresponding peaks, d_w^M, of the small energy barriers. While the profiles of the free energies and the corresponding global minima, ΔF_{min} (shown in Table 1), give a direct measure of the strength of dNMP's interaction with the walls, the scalar parameter, ΔF_{ads}, the so-called net free energy of adsorption, is more appropriate for a comparison with experiment.[45] From the free energy profile, we obtain the net free energy of adsorption, ΔF_{ads}, by evaluating the weighted sum of the free energies of all states characterizing dNMPs in the adsorbed state as

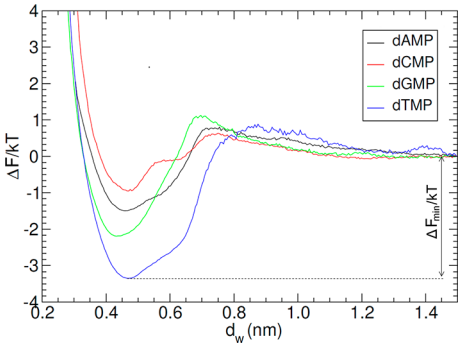

Figure 3. Free energies of the four dNMPs as a function of the distance from the hydrophobic walls, d_w. These curves are averages over all the different sets of wall configurations.

Table 1. Minima of the Free Energy Profiles (ΔF_{min}) for the Four dNMPs Interacting with the Hydrophobic Slit Walls and Their Average Free Energy of Adsorption, ΔF_{ads}, Together with the Position of the Free Energy Maxima (d_w^M) Used to Delimit the Adsorption Region[a]

dNMP	$\Delta F_{min}/kT$	$\Delta F_{ads}/kT$	d_w^M (nm)
dAMP	−1.6 ± 0.4	−0.69 ± 0.07	0.71 ± 0.09
dCMP	−1.0 ± 0.7	−0.21 ± 0.05	0.71 ± 0.05
dGMP	−2.2 ± 0.7	−1.19 ± 0.03	0.70 ± 0.04
dTMP	−3.4 ± 0.4	−2.62 ± 0.04	0.88 ± 0.03

[a]These values are averages over all the different sets of wall configurations. The calculation of uncertainties is described in the Supporting Information.

$$\Delta F_{ads} = -\ln\left(\frac{C_{ads}}{C_{bulk}}\right) = \int_0^{d_w^M} PD(d_w)\Delta F(d_w)\, d(d_w) \approx \sum_i PD_i \Delta F_i (\Delta d_w)_i = \sum_i Pr_i \Delta F_i \quad (2)$$

In this equation, ΔF_{ads} and ΔF are expressed in units of kT. C_{ads} is concentration in the adsorption region, and C_{bulk} is concentration in the bulk solution far from the walls. The subscript i denotes the bin number. $(d_w)_i$ is the location of bin i, which has a width of $(\Delta d_w)_i$. Pr_i represents the probability of the dNMP being in a given bin. $PD_i = Pr_i/(\Delta d_w)_i$ represents the normalized probability density in a given bin. Table 1 gives a summary of the relevant quantities characterizing the energetics and the extent of the adsorption regions of dNMPs adsorption to the slit hydrophobic walls.

Adsorption and Desorption Dynamics. Relating the adsorption and desorption statistical and dynamical properties to other properties such as flight times is of great interest. The analysis of the simulation results indicate that, while the dNMPs were adsorbed, the rings of the relatively hydrophobic nucleobases tended to be nearly flat on the surface, the hydrophilic phosphate groups pointed away from the surface, and the sugar also had some contact with the surface (see Figure 2). This hydrophobic adhesion of the nucleobases to a surface has been observed previously in simulations of transport of DNA strands through a silicon nitride nanopore[46] and with a graphene sheet in simulations of the transport of DNA strands though a graphene nanopore.[10] Figure 4 shows 50 ns segments of the z component of the trajectories of the center of mass of the dNMPs during flow simulations. Trajectories for equilibrium simulations are similar. There are clear differences between the trajectories of the four dNMPs as indicated by the differences in the frequency and the length of the adsorption events. In order to quantify the adsorption and desorption statistics, a methodology for determining adsorption and desorption times was introduced and is explained in detail in the Supporting Information.

The global minima and the small barriers in the PMF curves are related to the adsorption and desorption mechanism. Because the planar rings of the dNMPs tend to adsorb to the walls, the angles between two axes defined in the plane of the nucleobases and the wall surface planes are useful for looking at the adsorption/desorption mechanism. The average angles of an axis pointing from or near the atom in the nucleobase where

dx.doi.org/10.1021/jp309486c | J. Phys. Chem. B XXXX, XXX, XXX−XXX

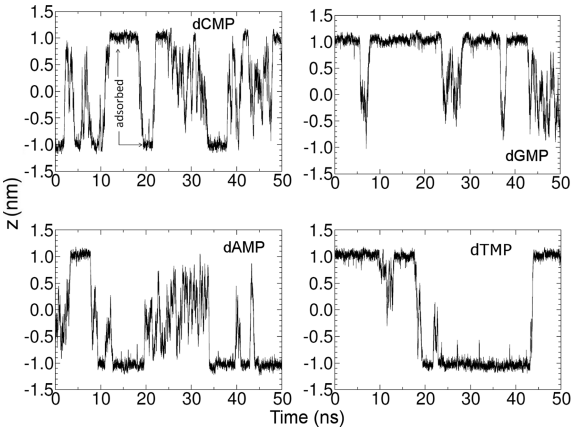

Figure 4. Typical 50 ns trajectories of the center of mass of the dNMPs in the z direction (perpendicular to the wall surfaces).

the sugar attaches to the other end of the nucleobase (axis 1) with the nearest wall surface plane as a function of d_w are shown in Figure 5 for adsorption and Figure 6 for desorption in both

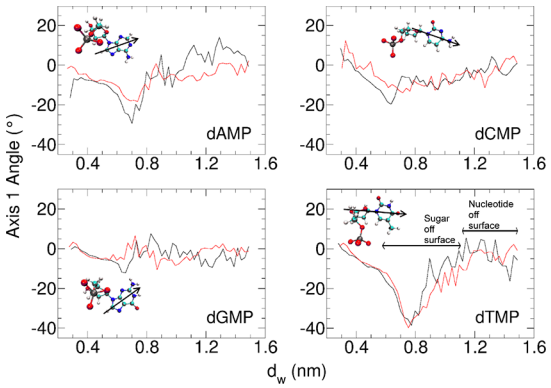

Figure 5. Angle of axis 1 with the surface plane as a function of d_w for adsorption in the equilibrium case (red) and nonequilibrium case (black). The arrows on the structures indicate the direction the axis points. Negative is pointing away from the center plane of the slit (d_w = 1.5 nm).

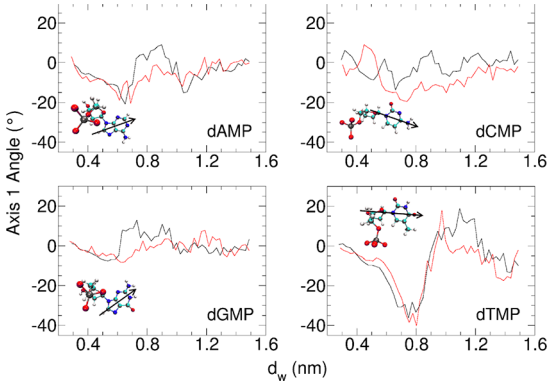

Figure 6. Angle of axis 1 with the surface plane as a function of d_w for desorption in the equilibrium case (red) and nonequilibrium case (black). The arrows on the structures indicate the direction the axis points. Negative is pointing away from the center plane of the slit (d_w = 1.5 nm).

the equilibrium and nonequilibrium cases. The average angles of an axis orthogonal to axis 1 and in the plane of the nucleobase (axis 2) with the nearest wall surface as a function of d_w were also calculated. In general, the angle of axis 2 did not change much during adsorption and desorption. These results are not crucial to the discussion of the adsorption and desorption mechanism; therefore, they can be found in the Supporting Information. Axis 1 is shown in Figure 1 as well as on the plot insets. For the purpose of calculating the average angles, the periods for adsorption were from halfway between the previous desorption time and a given adsorption time to halfway between that adsorption time and the next desorption time. A similar approach was used to determine desorption periods. Table 2 shows the average axis 1 angles calculated while the

Table 2. Average Axis 1 Angles with the Wall Surface (Degrees) while the dNMPs Are Adsorbed for the Equilibrium and Nonequilibrium Cases[a]

dNMP	equilibrium	nonequilibrium
dAMP	−8.60 ± 1.15	−9.00 ± 1.10
dCMP	−7.86 ± 1.33	−6.16 ± 3.25
dGMP	−4.63 ± 0.58	−4.37 ± 2.09
dTMP	−8.84 ± 0.93	−8.91 ± 0.66

[a]The uncertainties are 2 times the standard deviation of the mean, and their calculation is described in the Supporting Information.

dNMPs were adsorbed, regardless of whether this was during an adsorption or desorption period.

The curves in Figures 5 and 6 show that the ends of the nucleobases attached to the sugar adsorb last and desorb first. This is because the sugar and phosphate groups are more hydrophilic than the nucleobases, which more favorably interact with the hydrophobic slit walls. The magnitudes of the global minima in the axis 1 angles follow the same trend as the hydrophobicities of the nucleobases (G < C < A < T).[47,48] For the nucleobases that are closer in hydrophobicity to the sugar, the minimum in the axis 1 angle is not as severe. The minima in the PMF curves, around d_w = 0.475 nm, occurred when the sugar end of the nucleobase was slightly farther from the surface than the other end, but was still adsorbed. Detachment of the sugar end from the surface increases the free energy. The barriers in the PMF curves at $d_w = d_w^M$ (see Table 1) are associated with adsorption and desorption of the end of the nucleobase opposite the sugar end, which is the last part of the dNMP to leave the surface.

The adsorption and desorption curves for a given dNMP shown in Figures 5 and 6 for axis 1 are not identical. For dAMP, dCMP, and dGMP, the magnitudes of the global minima in the axis 1 angles were larger for desorption than for adsorption. For dTMP, the magnitude of the global minimum in the axis 1 angles was smaller for desorption than adsorption, and there was a significant maximum in the desorption curve. The larger magnitudes of the minima for dTMP were due to the hydrophobic methyl group sticking to the surface.

The angles of axis 1 with the wall surface usually have the same qualitative and often quantitatively very similar behavior in the nonequilibrium case compared to the equilibrium case. The exception in the qualitative behavior is that during desorption of the pyrimidine bases (dAMP and dGMP) there is a maximum in the nonequilibrium case, but not in the equilibrium case.

Role of dNMP Interaction with Channel Walls on Various Equilibrium and Flow Characteristics. Table 3 shows various quantities calculated from the simulations. These show, among others, that (i) for each of the four dNMPs the fraction of time adsorbed for the nonequilibrium case is nearly the same as in the equilibrium case. This is an indication that the adsorption/desorption behavior of the dNMPs is not significantly altered

dx.doi.org/10.1021/jp309486c | J. Phys. Chem. B XXXX, XXX, XXX−XXX

by the relatively high flow velocities used in our simulations. The flow velocities used are still small compared to the largest instantaneous thermal velocities of the molecules, which are on the order of hundreds of meters per second. (ii) The times of flight of dCMP and dTMP are well-separated even over only a 50 nm travel distance, meaning that an uncharged, hydrophobic surface, such as that used in these simulations, would certainly be sufficient to distinguish these two dNMPs. This can be attributed to differences in hydrophobicity of the nucleobases: G < C < A < T.[47,48] Thymine has a hydrophobic methyl group, whereas cytosine has a hydrophilic amine group. (iii) The increasing hydrophobicity trend matched the increasing time-of-flight trend except that the order of dGMP and dCMP was reversed. This was due to dNMP−wall interactions; the magnitude of the dGMP−wall energy ($V_{nuc-wall}$) while adsorbed was larger than the dCMP−wall energy while adsorbed. Because there are no strong specific interactions between different groups on the nucleobases and the wall surface and because the nucleobases sit nearly flat on the surface, $V_{nuc-wall}$ follows the same trend as the solvent-accessible surface area of the nucleobases (A_{base}). Because guanine has a larger area than cytosine, dGMP has a larger area in contact with the wall than dCMP and a larger $V_{nuc-wall}$. (iv) dAMP had twice as many adsorption events as did dGMP, but it was adsorbed for only a slightly smaller fraction of time and had a time of flight that was longer than that of dGMP. This resulted from the fact that dGMP spent longer stretches of time on or off the wall before desorbing or adsorbing again and that dGMP had a slightly larger wall sliding velocity. A comparison of the data shown in Table 3 with the data shown in Table 1 shows that the free energies calculated from equilibrium simulations show the expected trend, more negative minimum or average adsorption free energy gives a longer time of flight. The free energies for dGMP and dAMP are an exception to this.

Table 3. Quantities Calculated from the Flow Simulations, Except for the Last Three Rows[a]

dNMP	dCMP	dGMP	dAMP	dTMP
N_{sim} [b]	3	4	4	4
T_{sim} (ns)[c]	155.9	252.9	213.1	305.2
D (nm)[d]	50.0	48.0	32.0	32.0
n_{ads} [e]	0.21(0.06)	0.08(0.03)	0.18(0.03)	0.09(0.06)
$f_{ads,neq}$ [f]	0.38(0.15)	0.68(0.23)	0.63(0.10)	0.93(0.03)
t_{flight} (ns)[g]	52(7)	66(22)	77(19)	121(30)
v_{all} (m/s)[h]	0.99(0.23)	0.80(0.17)	0.63(0.18)	0.41(0.13)
v_{slide} (m/s)[i]	0.68(0.61)	0.42(0.24)	0.33(0.28)	0.38(0.14)
$V_{nuc-wall}/(kT)$ [j]	−10.9(0.4)	−14.5(0.3)	−13.2(0.3)	−12.4(0.2)
A_{base} (nm^2)[k]	2.4270	2.7963	2.6446	2.6197
$f_{ads,eq}$ [l]	0.38(0.09)	0.68(0.14)	0.60(0.05)	0.90(0.09)

[a]The area of the bases is from a single configuration, and the last two rows are from equilibrium simulations. Uncertainties in parentheses are 2 times the standard deviation of the mean, and their calculation is described in the Supporting Information. [b]Number of wall configurations (simulations). [c]Total simulation time for all configurations. [d]Distance traveled in the flow direction for each configuration. [e]Number of adsorption events per nanometer traveled. [f]Fraction of time adsorbed, nonequilibrium. [g]Time of flight over 50 nm distance. [h]Average velocity in the flow direction. [i]Average velocity in the flow direction while adsorbed. [j]dNMP−wall potential energy while adsorbed. [k]Solvent-accessible surface area of the nucleobases. [l]Fraction of time adsorbed, equilibrium.

Required Channel Length for Separation of dNMPs Based on the Nonequilibrium MD Simulations. The required channel length to achieve reliable separation of the times of flight of all four dNMPs was calculated from the distributions of the times of flight ($DTOF_{0.5}$) of dNMPs over 0.5 nm segments sampled from the total length of the corresponding MD trajectories. The total lengths of these trajectories are 128 nm for dTMP and dAMP, 150 nm for dCMP, and 192 nm for dGMP (see Table 3, rows 1 and 3). The choice of 0.5 nm for the length of the sampling segments is arbitrary, and our analysis indicates that using any other length between 0.5 and 50.0 nm gives approximately the same result. Using the $DTOF_{0.5}$ and employing the classical central limit theorem[49] one can calculate for each dNMP the distribution of the time of flight ($DTOF_{0.5N}$) over the larger distance, $d = 0.5N$ nm, where N is a positive integer number. For each dNMP using the $DTOF_{0.5}$ one can construct the corresponding $DTOF_{0.5N}$ as a function describing the distribution of the random variables $T_N = t_1 + t_2 + ... + t_N$, where $\{t_1, t_2, ..., t_N\}$ is a set of independent time-of-flight values t_i (i = 1, N), randomly drawn from $DTOF_{0.5}$. Each new random variable, T_N, represents a dNMP time of flight over $d = 0.5N$ nm. According to the central limit theorem, if μ and σ^2 are the mean and the variance, respectively, characterizing the $DTOF_{0.5}$, which needs not necessarily be a normal or even symmetric distribution, in the limit of large values of N the $DTOF_{0.5N}$ will approximate the normal distribution and will be characterized by the mean value $N\mu$ and by the variance $N\sigma^2$ (or standard deviation equal to $(N)^{1/2}\sigma$). As the number of segments N is increased the width of the $DTOF_{0.5N}$ increases only as the square root of N compared to the mean value which increases linearly with N. Therefore, the increase of N, which in this case translates in the increase of the distance of flight, leads to better separation of the $DTOF_{0.5N}$. Obviously, when estimating the required minimum channel length $d_{min} = 0.5N$ nm for separation one needs to define the acceptable level of distributions overlap. In our approach $d_{min} = 0.5N$ nm was estimated as the distance traveled by the dNMPs when N was such that less than 0.27% of any one of the distributions of the mean overlapped with one of the other distributions of the mean. This percentage corresponds to 3 standard deviations from the mean for a normal distribution. The misidentification rate for C and T would be 0.27%, and the rate for A and G would be 0.46%. The details on the calculation of N and the required length are given in the Supporting Information.

Table 4 shows the values of distances required to separate the time-of-flight distributions for each of the six different dNMP pairs. The length required to fully distinguish all of the dNMPs is 5.9 μm and represents the distance required to separate the times-of-flight distributions of dAMP and dGMP. Although this estimate was obtained for the conditions of the simulations which would be difficult to replicate in a real

Table 4. Distances (in Micrometers) Required to Separate the Times of Flight of dNMP Pairs

	dCMP	dGMP	dAMP	dTMP
dCMP	∞	1.31	0.43	0.06
dGMP	1.31	∞	**5.94**	0.24
dAMP	0.43	**5.94**	∞	0.56
dTMP	0.06	0.24	0.56	∞

dx.doi.org/10.1021/jp309486c | J. Phys. Chem. B XXXX, XXX, XXX−XXX

system, this number may be used as the basis for comparison of different surfaces. Figure 7 shows the time-of-flight distributions

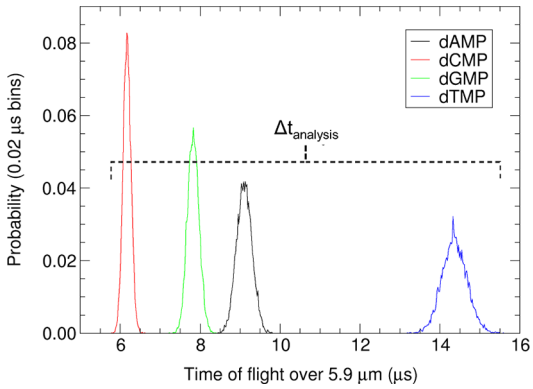

Figure 7. Flight time distributions over 5.9 μm. A total of 10 000 times of flight was used for each dNMP with each data point generated by summing up the times of flight of $N_{dAMP,dGMP}$ = 11 887 random samples from the flight time distributions over 0.5 nm. The minimum analysis time per dNMP ($\Delta t_{analysis}$) is about 10 μs.

over 5.9 μm with each time of flight generated by summing up $N = N_{dAMP,dGMP}$ samples from the 0.5 nm time-of-flight distributions. At this distance the distributions for dAMP and dGMP are just barely separated. The width of the whole set of distributions is the minimum analysis time per dNMP ($\Delta t_{analysis}$), since the time between dNMPs entering the channel must be at least this long in order to prevent misordering.

Estimate for Realistic Flow Rates. Although the dNMPs can be separated over a short distance on the order of micrometers with the minimum analysis time per dNMP on the order of 10 μs in the MD simulation, realistic flow rates will be 2−3 orders of magnitude smaller. Under those conditions, there will be significantly more broadening of the time-of-flight distributions due to diffusion. In this subsection, the effect of diffusion on the required channel length and the minimum analysis time per dNMP are estimated.

Perhaps the best way of estimating the effect of realistic flow rates, short of doing extremely expensive MD simulations at low flow rates, would be to use the strategy introduced by Carr et al.[44] which would involve calculating potentials of mean force (PMF) between the dNMPs and the walls in all three Cartesian dimensions and then using the resulting forces as a function of position in Brownian dynamics (BD) simulations. Although the forces derived from an equilibrium PMF calculation are not strictly correct under nonequilibrium conditions, Carr et al.[44] showed that there was good agreement between BD simulations and MD simulations with pressure-driven flow. The advantage of this 3D PMF + BD strategy would be that, although the PMF calculation would be expensive, the BD simulations would involve only a single dNMP which would allow for much larger time scales and channel widths compared to MD simulations.

Using some assumptions about the diffusivities and velocity profiles of the dNMPs and the probability of observing the dNMPs as a function of distance from the walls which is related to the PMFs by eq 1, order of magnitude channel lengths and analysis times per dNMP can be obtained without having to calculate a 3D PMF. The following assumptions were used:

(1) The diffusivities of all of the dNMPs at any distance from the walls are the same and equal to the diffusivity of cyclic AMP which is 4.44 × 10^{-6} cm^2/s.[50]

(2) The velocity profile of the dNMPs is parabolic with a maximum velocity (v_{max}) of 0.048 cm/s, which is about the speed that the dNMPs would travel by electrophoresis in bulk aqueous solution under an electric field of 1000 V/cm, and a velocity of zero for values of d_w less than or equal to the average dNMP position while adsorbed. Assuming zero sliding velocity is probably not correct, but at lower velocities and with rougher walls the ratio of sliding velocity to average velocity will be much lower than in the MD simulations. Assuming a different shape of the velocity profile would alter the average velocities somewhat, but not change the order of magnitude of the estimates.

(3) The average velocity in the flow direction (x) is

$$\bar{v}_x = \int_0^{d_w^{CL}} PD(d_w) v_x(d_w)\, d(d_w) \approx \sum_i PD_i v_{x,i}(\Delta d_w)_i = \sum_i Pr_i v_{x,i} \quad (3)$$

This is similar to eq 2 and uses the same symbols except for $v_{x,i}$, which is the velocity in the flow direction in bin i, and d_w^{CL}, which is the distance from the walls at the center line of the slit. The use of eq 3 assumes that the probabilities are the same in the flow situation as in the equilibrium simulation. Given that even in the nonequilibrium MD simulations at very high velocity the fractions of time adsorbed were similar, this is a valid assumption.

(4) For a given channel length L, average velocity $\bar{v}_x$, and diffusivity D, the time-of-flight probability density distribution is

$$\rho(t) = \frac{1}{\sqrt{4\pi D t}} \exp\left[\frac{-(L - \bar{v}_x t)^2}{4Dt}\right] \quad (4)$$

which is just the distribution for one-dimensional diffusion with a time-dependent average position of $\bar{v}_x t$.

(5) The allowed overlap of distributions was the same as used in the analysis of the MD simulations.

With these assumptions in place, the goal was to find the minimum L that did not violate the desired overlap of distributions and the corresponding $\Delta t_{analysis}$. The values of L and $\Delta t_{analysis}$ determined for v_{max} = 0.048 cm/s were estimated to be about 2.5 mm and 39 s, respectively. Figure 8 shows the

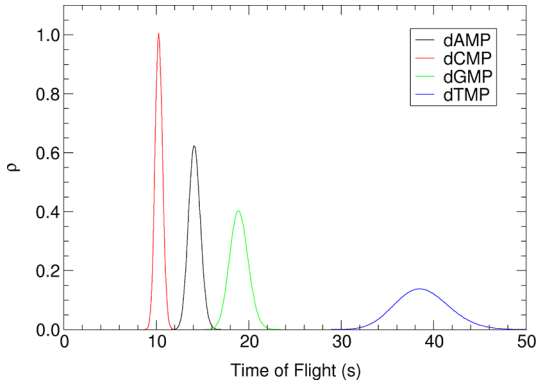

Figure 8. Estimated time-of-flight distributions for a center line velocity (v_{max}) of 0.048 cm/s and a channel length of 2.47 mm.

time-of-flight distributions over the 2.5 mm distance. Although channels with sub-20 nm dimensions of up to 1 cm long have

dx.doi.org/10.1021/jp309486c | J. Phys. Chem. B XXXX, XXX, XXX−XXX

been fabricated,[51] the time to analyze each dNMP is too long considering that millions or billions of dNMPs (the human genome has about 3 billion base pairs) might need to be sequenced. Sequencing the human genome in a day at that rate would require about 1.4 million channels in parallel, not including any redundancy. Fortunately, while L is only inversely proportional to the velocity, $\Delta t_{analysis}$ is inversely proportional to the velocity squared. If the velocity was increased by a factor of 10, the required length would be 250 μm and $\Delta t_{analysis}$ would be 390 ms.

For a given v_{max}, there is a minimum possible $\Delta t_{analysis}$ which can be estimated. In addition to assumptions 1,4, and 5 above, one of the dNMP types is assumed to have $\overline{v}_{x,1} = v_{max}$; it is assumed to not be affected by the walls. A second dNMP type is assumed to have $\overline{v}_{x,2} = \overline{v}_{x,2} - \Delta v_x$, and the third and fourth types to have even smaller velocities ($\overline{v}_{x,4} < \overline{v}_{x,3} < \overline{v}_{x,2}$) such that all of the distributions are crowded against each other as far as possible given assumption 5 above. By varying Δv_x, a minimum for $\Delta t_{analysis}$ can be found. For v_{max} = 0.048 cm/s, the minimum $\Delta t_{analysis}$ is about 5.0 s and L is about 1.29 mm. For v_{max} = 0.48 cm/s, the minimum $\Delta t_{analysis}$ is about 50 ms and L is about 129 μm.

CONCLUSIONS

The four deoxydNMP 5′-monophoshates commonly found in DNA were simulated in aqueous solution in 3 nm wide nanoslits composed of disordered Lennard-Jones carbon atoms in order to compare their times of flight and dynamics. The solution was driven by body forces, which are known to induce flow that is similar to that induced by pressure difference or capillary forces. For comparison, and to calculate the free energy for adsorbing the dNMPs onto the slit walls, a case with no external forces was also considered. The dNMPs adsorb and desorb within nanoseconds even with no flow. The flow did not have a large effect on the adsorption and desorption behavior of the dNMPs, and the fractions of time that the dNMPs were adsorbed were nearly the same in equilibrium and nonequilibrium simulations. The times of flight of the most hydrophobic dNMP (dTMP) and one of the most hydrophilic dNMP (dCMP) were easily separated using hydrophobic carbon slit walls, indicating that modifying the wettability properties of the wall material may be a promising way to achieve high reliability in discriminating between dNMPs on the basis of their flight times through nanochannels, although interactions of specific chemical groups in dAMP and dGMP with groups on the wall surface will also be important for their separation since their times of flight were nearly the same. Important questions regarding dAMP and dGMP are whether their qualitatively different behavior during desorption under flow conditions compared to equilibrium conditions plays a role in the ability to separate their times of flight and whether this behavior persists at the much lower velocities that would be used in a real device. Analysis of the effect of diffusion at realistic flow rates indicates that the dNMP velocity should be relatively high in order to get a reasonable minimum analysis time per dNMP.

ASSOCIATED CONTENT

Supporting Information

The CHARMM patch for the dNMPs with nonprotonated phosphate groups on the 5′ ends, definition of the algorithm for detection of dNMP adsorption and desorption events, the details on uncertainty estimates, the axis 2 angle results, and the details on the calculation of the required channel length. This material is available free of charge via the Internet at http://pubs.acs.org.

AUTHOR INFORMATION

Corresponding Author

*Phone: 225-578-6488. Fax: 225-578-5924. E-mail: dmoldo1@lsu.edu.

Notes

The authors declare no competing financial interest.

ACKNOWLEDGMENTS

This study is based upon work supported by National Science Foundation (Grant No. EPSCoR LA-SiGMA EPS-1003897, Grant No. EPSCoR EPS-0346411, and Grant No. CBET-1067583). Computer Resources were provided by LONI and HPC@LSU.

REFERENCES

(1) Deamer, D. W.; Branton, D. *Acc. Chem. Res.* **2002**, *35*, 817−825.
(2) Lagerqvist, J.; Zwolak, M.; Di Ventra, M. *Nano Lett.* **2006**, *6*, 779−782.
(3) He, Y. H.; Shao, L. B.; Scheicher, R. H.; Grigoriev, A.; Ahuja, R.; Long, S. B.; Ji, Z. Y.; Yu, Z. A.; Liu, M. *Appl. Phys. Lett.* **2010**, *97*, 3.
(4) McNally, B.; Singer, A.; Yu, Z. L.; Sun, Y. J.; Weng, Z. P.; Meller, A. *Nano Lett.* **2010**, *10*, 2237−2244.
(5) Sigalov, G.; Comer, J.; Timp, G.; Aksimentiev, A. *Nano Lett.* **2008**, *8*, 56−63.
(6) Luan, B. Q.; Peng, H. B.; Polonsky, S.; Rossnagel, S.; Stolovitzky, G.; Martyna, G. *Phys. Rev. Lett.* **2010**, *104*, 4.
(7) Clarke, J.; Wu, H. C.; Jayasinghe, L.; Patel, A.; Reid, S.; Bayley, H. *Nat. Nanotechnol.* **2009**, *4*, 265−270.
(8) Rhee, M.; Burns, M. A. *Trends Biotechnol.* **2006**, *24*, 580−586.
(9) Schneider, G. F.; Kowalczyk, S. W.; Calado, V. E.; Pandraud, G.; Zandbergen, H. W.; Vandersypen, L. M. K.; Dekker, C. *Nano Lett.* **2010**, *10*, 3163−3167.
(10) Wells, D. B.; Belkin, M.; Comer, J.; Aksimentiev, A. *Nano Lett.* **2012**, *12*, 4117−4123.
(11) Nelson, T.; Zhang, B.; Prezhdo, O. V. *Nano Lett.* **2010**, *10*, 3237−3242.
(12) Merchant, C. A.; Healy, K.; Wanunu, M.; Ray, V.; Peterman, N.; Bartel, J.; Fischbein, M. D.; Venta, K.; Luo, Z. T.; Johnson, A. T. C.; et al. *Nano Lett.* **2010**, *10*, 2915−2921.
(13) Garaj, S.; Hubbard, W.; Reina, A.; Kong, J.; Branton, D.; Golovchenko, J. A. *Nature* **2010**, *467*, 190−193.
(14) Siwy, Z. S.; Davenport, M. *Nat. Nanotechnol.* **2010**, *5*, 697−698.
(15) Bayley, H. *Nature* **2010**, *467*, 164−165.
(16) Postma, H. W. C. *Nano Lett.* **2010**, *10*, 420−425.
(17) Prasongkit, J.; Grigoriev, A.; Pathak, B.; Ahuja, R.; Scheicher, R. H. *Nano Lett.* **2011**, *11*, 1941−1945.
(18) Davis, L. M.; Fairfield, F. R.; Harger, C. A.; Jett, J. H.; Keller, R. A.; Hahn, J. H.; Krakowski, L. A.; Marrone, B. L.; Martin, J. C.; Nutter, H. L.; et al. *Genet. Anal.: Biomol. Eng.* **1991**, *8*, 1−7.
(19) Goodwin, P. M.; Cai, H.; Jett, J. H.; IshaugRiley, S. L.; Machara, N. P.; Semin, D. J.; VanOrden, A.; Keller, R. A. *Nucleosides Nucleotides* **1997**, *16*, 543−550.
(20) Werner, J. H.; Cai, H.; Jett, J. H.; Reha-Krantz, L.; Keller, R. A.; Goodwin, P. M. *J. Biotechnol.* **2003**, *102*, 1−14.
(21) Eid, J.; Fehr, A.; Gray, J.; Luong, K.; Lyle, J.; Otto, G.; Peluso, P.; Rank, D.; Baybayan, P.; Bettman, B.; et al. *Science* **2009**, *323*, 133−138.
(22) Czarnecka, J.; Cieslak, M.; Michal, K. *J. Chromatogr., B: Anal. Technol. Biomed. Life Sci.* **2005**, *822*, 85−90.
(23) Inoue, K.; Obara, R.; Akiba, T.; Hino, T.; Oka, H. *J. Agric. Food Chem.* **2008**, *56*, 6863−6867.
(24) Perrett, D.; Bhusate, L.; Patel, J.; Herbert, K. *Biomed. Chromatogr.* **1991**, *5*, 207−211.

(25) Wu, J. H.; Chantiwas, R.; Amirsadeghi, A.; Soper, S. A.; Park, S. *Lab Chip* **2011**, *11*, 2984−2989.
(26) Chantiwas, R.; Hupert, M. L.; Pullagurla, S. R.; Balamurugan, S.; Tamarit-Lopez, J.; Park, S.; Datta, P.; Goettert, J.; Cho, Y. K.; Soper, S. A. *Lab Chip* **2010**, *10*, 3255−3264.
(27) Henry, A. C.; Tutt, T. J.; Galloway, M.; Davidson, Y. Y.; McWhorter, C. S.; Soper, S. A.; McCarley, R. L. *Anal. Chem.* **2000**, *72*, 5331−5337.
(28) McCarley, R. L.; Vaidya, B.; Wei, S. Y.; Smith, A. F.; Patel, A. B.; Feng, J.; Murphy, M. C.; Soper, S. A. *J. Am. Chem. Soc.* **2005**, *127*, 842−843.
(29) Soper, S. A.; Henry, A. C.; Vaidya, B.; Galloway, M.; Wabuyele, M.; McCarley, R. L. *Anal. Chim. Acta* **2002**, *470*, 87−99.
(30) Chou, S. Y.; Krauss, P. R.; Zhang, W.; Guo, L. J.; Zhuang, L. *J. Vac. Sci. Technol., B* **1997**, *15*, 2897−2904.
(31) Tsutsui, M.; Taniguchi, M.; Yokota, K.; Kawai, T. *Nat. Nanotechnol.* **2010**, *5*, 286−290.
(32) Plimpton, S. *J. Comput. Phys.* **1995**, *117*, 1−19.
(33) Foloppe, N.; MacKerell, A. D. *J. Comput. Chem.* **2000**, *21*, 86−104.
(34) Yeh, I. C.; Berkowitz, M. L. *J. Chem. Phys.* **1999**, *111*, 3155−3162.
(35) *Nucleic Acids in Chemistry and Biology*; Blackburn, G. M., Gait, M. J., Eds.; IRL Press: Oxford, U.K., 1990.
(36) Sane, S. B.; Cagin, T.; Knauss, W. G.; Goddard, W. A. *J. Comput.-Aided Mater. Des.* **2002**, *8*, 87−106.
(37) Menard, L. D.; Ramsey, J. M. *Nano Lett.* **2011**, *11*, 512−517.
(38) Humphrey, W.; Dalke, A.; Schulten, K. *J. Mol. Graphics* **1996**, *14*, 33−38.
(39) Zhu, F. Q.; Tajkhorshid, E.; Schulten, K. *Biophys. J.* **2002**, *83*, 154−160.
(40) Carr, R.; Comer, J.; Ginsberg, M. D.; Aksimentiev, A. *IEEE Trans. Nanotechnol.* **2011**, *10*, 75−82.
(41) Han, A.; Mondin, G.; Hegelbach, N. G.; de Rooij, N. F.; Staufer, U. *J. Colloid Interface Sci.* **2006**, *293*, 151−157.
(42) Torrie, G. M.; Valleau, J. P. *Chem. Phys. Lett.* **1974**, *28*, 578−581.
(43) Carr, R.; Comer, J.; Ginsberg, M. D.; Aksimentiev, A. *J. Phys. Chem. Lett.* **2011**, *2*, 1804−1807.
(44) Carr, R.; Comer, J.; Ginsberg, M. D.; Aksimentiev, A. *Lab Chip* **2011**, *11*, 3766−3773.
(45) Raut, V. P.; Agashe, M. A.; Stuart, S. J.; Latour, R. A. *Langmuir* **2005**, *21*, 1629−1639.
(46) Aksimentiev, A.; Heng, J. B.; Timp, G.; Schulten, K. *Biophys. J.* **2004**, *87*, 2086−2097.
(47) Shih, P.; Pedersen, L. G.; Gibbs, P. R.; Wolfenden, R. *J. Mol. Biol.* **1998**, *280*, 421−430.
(48) Munoz-Muriedas, J.; Barril, X.; Lopez, J. M.; Orozco, M.; Luque, F. J. *J. Mol. Model.* **2007**, *13*, 357−365.
(49) Wasserman, L. W. *All of Statistics: A Concise Course in Statistical Inference*; Springer-Verlag: New York, 2004.
(50) Dworkin, M.; Keller, K. H. *J. Biol. Chem.* **1977**, *252*, 864−865.
(51) Liang, X. G.; Morton, K. J.; Austin, R. H.; Chou, S. Y. *Nano Lett.* **2007**, *7*, 3774−3780.